NUMERICAL SIMULATION OF SOUND GENERATION AND PROPAGATION IN AND OUTSIDE A CABIN AIR INTAKE

M. Konstantinov and C. Wagner
German Aerospace Center, Institute of Aerodynamics and Flow Technology,
Bunsenstrasse 10, D-37073 Göttingen, Germany
mikhail.konstantinov@dlr.de

Abstract

Aerodynamic noise generated by the low Mach number flow in an air cabin intake is investigated numerically. For analysis a realistic intake installed DLR's cabin test facility Do728, was chosen. Two independent approaches were used. First, the so called hybrid approach, based an incompressible simulation of the airflow in the intake and Lighthill aeroacoustical analogy was applied, which separates generation and propagation of sound. The flow field was calculated with OpenSource code OpenFOAM and acoustical sources and sound waves propagation were computed with commercial program Virtual.Lab. Second, the flow and acoustical field were computed in a Computational Aero Acoustics calculation (CAA) with the Star-CCM+ code. The latter simulates both the unsteady turbulent flow and the noise it generates. The results from both calculations were compared and discussed.

1. INTRODUCTION

The prediction of passengers comfort in the aircraft cabin depends among other things on the prevailing noise level. In addition to engine and boundary layer noise also the sound, which arise in the air conditioning system and get from there in the cabin, contributes to the overall noise level The aim of our study is to predict the sound generation and propagation simulating the turbulent flows in a realistic cabin air intake of the Do728 together with computational aero acoustics (CAA) predictions. The prediction of sound propagation is closely related to the calculation of flow and turbulence modeling. Aircraft climate systems typically exhibit aeroacoustic noise which is closely related to turbulence and vortex shedding. For designer necessary knowledge of absolute dB levels and relative magnitude of modal frequencies are obtainable via direct experimentation or simulation. The large Eddy simulation (LES) enables a reliable prediction of turbulent fluctuations, allowing an identification of the sound sources. Often the Detached Eddy is used for in industry issues simulation (DES), which essentially represents a combination of RANS and LES.

This paper exploits the substantial potential of aeroacoustics simulation in the context of cabin air intake, a typical component used in aircraft climate system. The numerical approach has the clear benefit of reducing the need for experimental rigs, and potentially provides far greater insight into the flow phenomena involved. Acoustic modeling has been carried with CFD/CAA code Star-CCM+ and coupling between CFD code OpenFOAM and CAA code Virtual.Lab. The simulation process combines a LES flow simulation with the prediction of noise propagation from a CAA calculation.

2. MODELING AEROACOUSTICS

The mass and momentum conservation equations governing the motion of fluid can be written as

$$(1)\quad \frac{\partial \rho}{\partial t} + \frac{\partial}{\partial x_i}\left(\rho v_i\right) = 0$$

$$(2)\quad \frac{\partial}{\partial t}\left(\rho v_i\right) + \frac{\partial}{\partial x_j}\left(\rho v_i v_j\right) = -\frac{\partial p}{\partial x_i} + \frac{\partial \tau_{ij}}{\partial x_i},$$

where ρ is fluid density, $\boldsymbol{v}$ is the velocity, p is the pressure and $\boldsymbol{\tau}$ is the viscous stress tensor.

Lighthill [1] proposed to derive from exact equations of mass (1) and momentum conservation (2) a nonhomogeneous wave equation that reduces to the homogeneous wave equation in a region surrounding the listener. By combination of Eqs. (1) and (2), Lighthill's analogy is found as

$$(3)\quad \frac{\partial^2}{\partial t^2}\left(\rho - \rho_0\right) - a_0^2 \frac{\partial^2}{\partial x_i \partial x_j}\left(\rho - \rho_0\right) = \frac{\partial^2 T_{ij}}{\partial x_i \partial x_j},$$

where ρ_0 denotes the density at rest, a_0 the speed of sound at rest and **T** is the Lighthill's tensor defined as

$$(4)\quad T_{ij} = \rho v_i v_j + \left(\left(p - p_0\right) - a_0^2\left(\rho - \rho_0\right)\right)\delta_{ij} - \tau_{ij}.$$

For the high Reynolds number and low Mach number flow, Lighthill's tensor **T** can be approximated by

$$(5)\quad T_{ij} \approx \rho_0 v_i v_j.$$

In presence of solid walls the integral formulation of Lighthill's analogy was first derived by Curle [2] assumes a

fixed control surface. Later Ffowcs Williams and Hawkings [3] and Möhring, Müller and Obermeier [4] independently generalized Curle's equation to include bodies with arbitrarily moving boundaries. As the integral representations of the sound field in these theories were based on free-space Green's functions, the include volume integrals as well as surface integrals. The so-called Ffowcs Williams – Hawkings (FW-H) equation is an exact rearrangement of the continuity and the momentum equations into the form of an inhomogeneous wave equation. The FW-H equation gives accurate results even if the surface of integration lies in the nonlinear flow region. It is based on the free-space Green's function to compute the sound pressure at the observer location, *x*. The FW-H equation for pressure that radiated into a medium at rest by a flow in a region or set of surfaces is

$$(6)\quad p'(\vec{x},t) = p'_T(\vec{x},t) + p'_L(\vec{x},t) + p'_Q(\vec{x},t).$$

The monopole term $p'_T(\vec{x},t)$ is

$$(7)\quad p'_T(\vec{x},t) = \frac{1}{4\pi}\left(\left(-\frac{\partial}{\partial t}\right)\int_S\left[\frac{Q}{(r(1-M_r))}\right]_{ret} dS\right),$$

the dipole term $p'_L(\vec{x},t)$ --

$$(8)\quad p'_L(\vec{x},t) = \frac{1}{4\pi}\left(\left(-\frac{\partial}{\partial x_i}\right)\int_S\left[\frac{L_i}{(r(1-M_r))}\right]_{ret} dS\right)$$

and the quadrupole term $p'_Q(\vec{x}.t)$ is:

$$(9)\quad p'_Q(\vec{x},t) = \frac{1}{4\pi}\left(\left(-\frac{\partial^2}{\partial x_i \partial x_j}\right)\int_V\left[\frac{T_{ij}}{(r(1-M_r))}\right]_{ret} dV\right)$$

with $Q = \rho_0 U_i n_i$; $U_i = \left(1-\frac{\rho}{\rho_0}\right)v_i + \frac{\rho u_i}{\rho_0}$;

$L_i = P_{ij}n_i + \rho u_i(u_n - v_n)$ and $P_{ij} = (p-p_0)\delta_{ij} - \sigma_{ij}$,

$r = x_{observer} - y_{face}$, where u_i represents fluid velocity components in the x_i direction; u_n is the fluid velocity component normal to surface; v_i represents surface velocity components; v_n is the surface velocity component normal to the surface; n_i is the surface normal vector; σ_{ij} is the viscous stress tensor; ρ_0 is the far field density; M_r is the Mach number of the source towards the observer; P_{ij} - the compressive stress tensor and T_{ij} - the Lighthill stress tensor.

The space derivatives from Eqs. (8) and (9) are transformed into time derivatives and afterwards, the time derivatives at the observer locations are moved into the integrals. Detailed theoretical description of CAA calculation can be found in [5].

3. NUMERICAL SETUP

The flow through upper cabin air intakes of the Do728 has been studied. Fig. 1 shows the inner geometry of cabin air intake reflecting a long flapper and several small channels that have a honeycomb structure. The size of the intake is 0.12 x 0.32 x 0.09 m^3.

A numerical mesh was created with Program StarCCM+. The CFD model consists of 6 Mio cells and 3.5 Mio vertices and takes into account the cabin air intake and the opening anechoic box (0.3 x 0.845 x 0.15 m^3). The CFD mesh and their vertical cross-section are presented in Fig. 2.

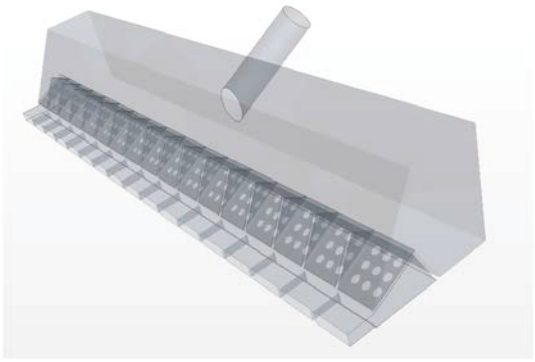

FIGURE 1: Sketch of cabin air intake of Do728

3.1. CFD and CAA simulation with StarCCM+

The StarCCM+ calculations were curried-out with DES-based SST (Menter) k – ω turbulence model for weak compressible low Mach number flow. Four types of boundary conditions are used. The first condition is a no-slip velocity condition at walls. At the inlet a mass flow is prescribed. Flow outlet condition is used at the outlet. At the anechoic box a symmetry plane condition is given.

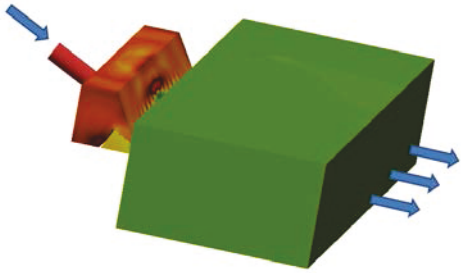

a) CFD Model

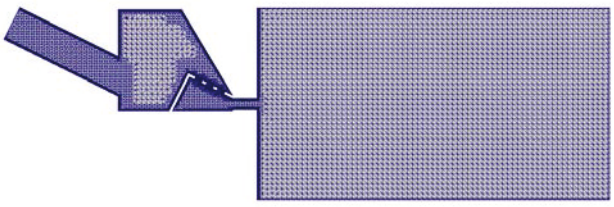

b) CFD Mesh (cross-section representation)

FIGURE 2: Computation CFD region: a) CFD Model; b) Cross-section of CFD Mesh

Different steps are needed before starting acquisition of data to be used by acoustic simulation. First, a steady state RANS simulation is performed. The aim of this step is to provide an initial condition for the subsequent transient simulations and to understand the important features of the flow and validate preliminary guess. The DES calculations were started from steady state solution. Time step of δt = 2.5e-5 s was chosen. The total elapsed time was t = 0.3 *s* for these calculations. The acoustical information has been stored at each time step. The FW-H surfaces (cabin air intake) and receiver points are defined. The FW-H solver allowed to calculation both dipole and quadrupole sources.

3.2. Coupling OpenFOAM and Virtual.Lab

A Large Eddy Simulation using a k-equation eddy viscosity subgrid scale turbulence model was performed with the CFD code OpenFOAM. We prescribed the same boundary conditions as in the StarCCM+ calculation with the exception of the outlet, where advective boundary condition was applied for the LES. The calculations were carried out for both incompressible and weak compressible flow for a time step of 1e-6 *s*, flow fields have been stored in time intervals of 5e-5 s and the acoustic analysis time interval of 0.1 *s*. Thus, a frequency of less than 10 *Hz* was resolved.

The velocity and pressure fields were exported over a time period of 0.1 s with the OpenFOAM operation 'Extract Surface' and subsequently 'Integrate Variables' in a total of 2000 csv-files. Then the created files were convert in Ideas*.unv-Format.

The CAA acoustic model consists of two parts (Fig. 3):

- Boundary Element (BEM) acoustic mesh (surface of cabin air intake);
- Field Point acoustic mesh (region for computation of sound propagation).

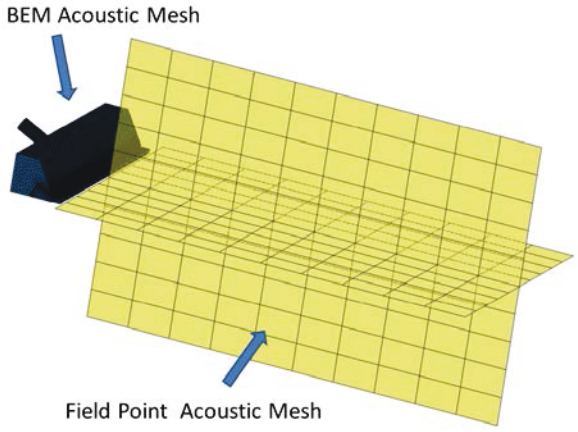

FIGURE 3: Acoustic meshes for calculation with Virtual.Lab

The CFD surface pressure data (from the fine CFD mesh) have been mapped with a conservative mapping algorithm on the coarse acoustic mesh. Then a Fast-Fourier-Transform (FFT) was performed. Afterwards surface dipole boundary conditions (distributes dipole on acoustic mesh) were defined and by solving the acoustic response case with the Field Point acoustic mesh was updated. In Virtual.Lab, it is possible to analyze both the incompressible and the compressible flow solutions. For incompressible flows, the hydrodynamic fluctuations on the surfaces are captured. The drawback is that the acoustic effect (acoustic reflection, scattering and propagation inside the air intake) are missed. Therefore, it is important to correct for that and make sure these acoustic effects are accounted for with the source modeling. By transforming the dipole sources into equivalent velocity boundary conditions, such effects are accounted for leading to more accurate predictions. Note that the analysis with Virtual.Lab is based on surface sources (dipole) only. Thus, it is assumed that the sources in the flow volume (quadrupoles) are negligible compared to the dipoles sources for low Mach number applications. At the end of the calculations a displayed resulting pressure on the Field Point mesh visualize, how acoustic energy is radiated through outlet of the cabin air intake. Further, for each point on field acoustic point mesh a calculation of Sound Pressure Level (SPL) spectra is possible.

The aeroacoustic simulation based on the hybrid approach by coupling between CFD (STAR-CD or ANSYS) and acoustics program Virtual.Lab or ACTRAN for HVAC system in passenger car are described in many papers, for example in [6-8]. Though, these results do not answer the questions addressed in the here presented paper, because aircraft air intake design concept.

4. COMPUTED FLOW FIELDS

Two flow situations were considered. At first, the flow with volume rate of 0.0068 m^3/s (correspond to mean inlet velocity at intake duct of 10 *m/s*), and second, the flow with double flow rate of 0.0136 m^3/s (mean velocity 20 *m/s*). Additional, OpenFOAM simulations were performed both for an incompressible and a compressible fluid. Further, the influence of CFD mesh quality was examined.

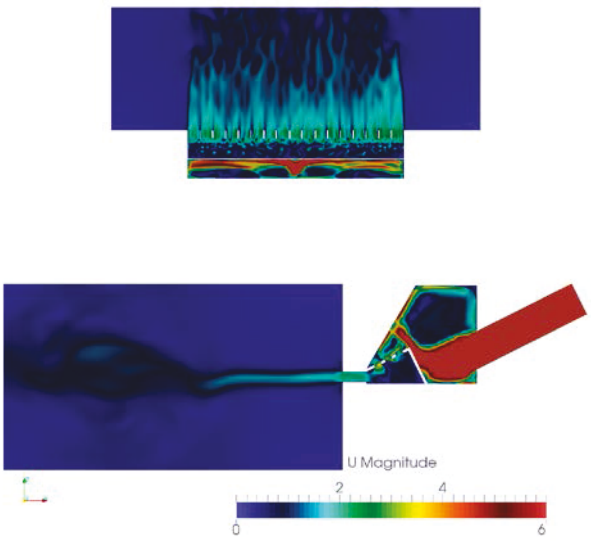

FIGURE 4: Snapshot of velocity distribution in horizontal and vertical planes

In the Fig. 4 the velocity distribution in vertical and horizontal planes for the case of mean inlet velocity 10 *m/s* is presented. In this situation, the outlet velocity from air intake reaches a value of 2 *m/s*.

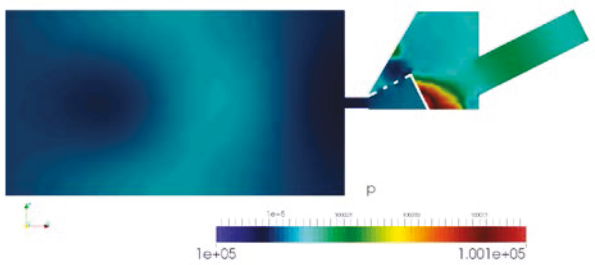

FIGURE 5: Pressure distribution in vertical plane

Additionally, the pressure distribution in the vertical plane of air intake is shown in Fig. 5 for the same time instant. The main pressure sources develop at the locations where the flow hits the flapper. The other relevant acoustical source is located at the front of the air intake.

Transient CFD calculations permit to compute a sound pressure level by FFT analysis for predefined points on the intake surface. In Fig. 6 the SPL spectra for monitor surface point p2 for case 1 (mean inlet velocity 10 *m/s*) and case 2 (mean inlet velocity 20 *m/s*) are presented.

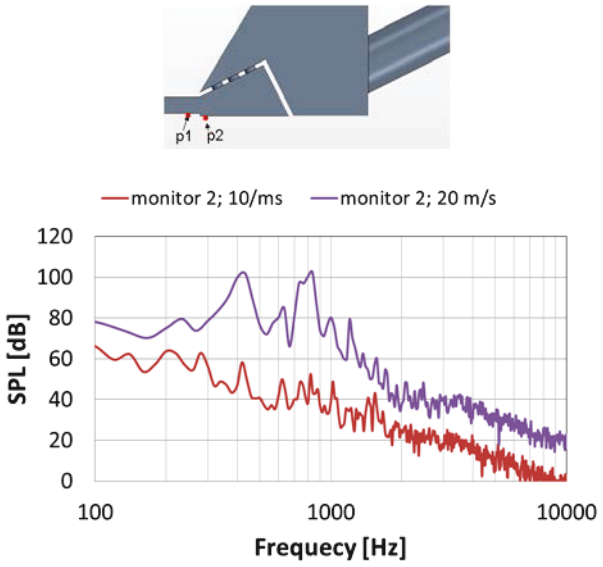

FIGURE 6: SPL Spectra from wall pressure perturbations at point p2 for case 1 (red) and case 2 (blue)

5. PREDICTED SOUND PROPAGATION

As mentioned above, OpenFOAM simulations were performed for both, incompressible and compressible fluid. For the incompressible case the correction for dipole sources by acoustic response was analyzed with in Virtual.Lab. The dipole sources were determined wit FFT at the intake surface for various frequencies. One example of radiated noise from air intake in far-field at 880 *Hz* for case 1 (inlet 10 *m/s*) for compressible flow, shown in Fig. 7, reveals the distribution of pressure amplitude in dB for top and site view.

Fig. 8 shows the radiated noise obtained for case 1 (compressible) and for three different characteristic frequencies. For all cases a weak signal at the displacement of 1 m from intake was observed. At the three yellow points, the Sound Pressure Level are analyzed and compared with StarCCM+ results of FW-H integral calculations. Note, that leads Direct Noise Simulation for predefined points. Point 1 is located close to the to intake outlet (displacement δr = 0.003 *m*), point 2 (δr = 0.3 *m*) at the end of the computational domain and there is a distance of 1 m between point 3 and the air intake.

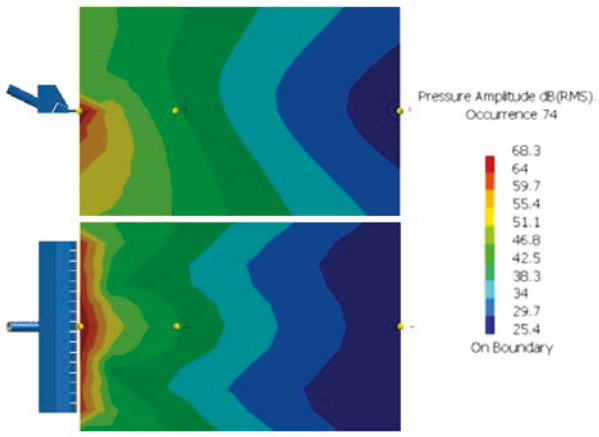

FIGURE 7: Sound radiated from air intake at 880 *Hz* for case 1 (compressible) in vertical and horizontal plane

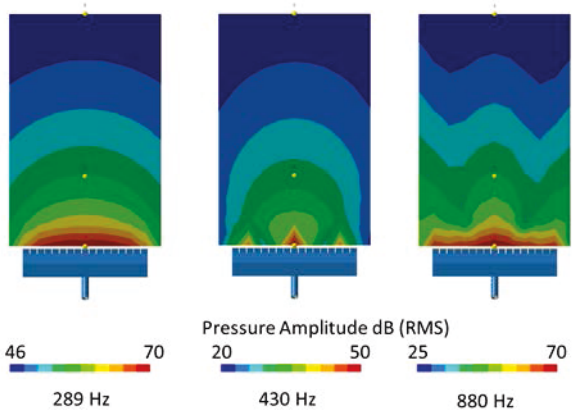

FIGURE 8: Far-field sound radiation for case 1 (compressible) at 289, 430 and 880 *Hz*

The next Fig. 9 shows the sound pressure distribution computed with StarCCM+ for 860 Hz and case 1. The instantaneous pressure data were saved every time step

and further evaluated with FFT. The results represent a wave structure of propagated sound.

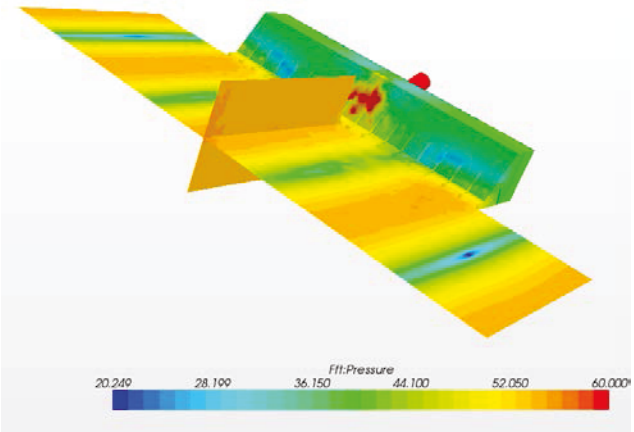

FIGURE 9: Distribution of FFT pressure in CFD domain at 860 Hz: StarCCM+

In Figs. 10 and 11 an effect of compressibility for SPL spectra at point 2 and at point 3 by calculations of sound propagation with Virtual.Lab (VL) for case 1 is presented. These spectra are compared with compressible StarCCM+ results.

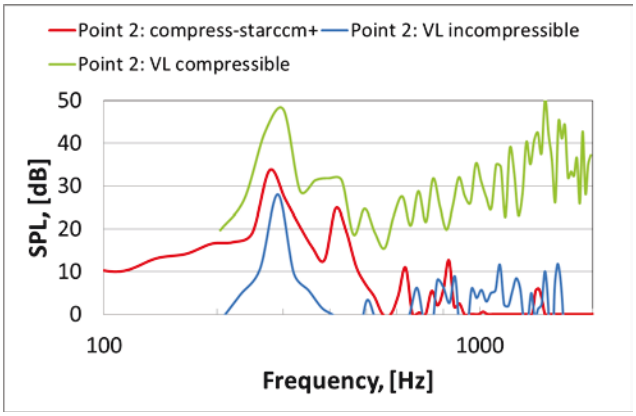

FIGURE 10: SPL spectra at point 2 for case 1: VL incompressible (blue); VL compressible (green); StarCCM+ compressible (red)

For both points an overall trend is observed: incompressible VL data with correction are lower than compressible VL results.

The difference between the solutions based on the incompressible and compressible approach was observed by studying a flow in controlling air craft duct [9]. Numerical Simulations indicate that feedback mechanism between flow wall interaction, vortex separation and the generated sound waves are not negligible.

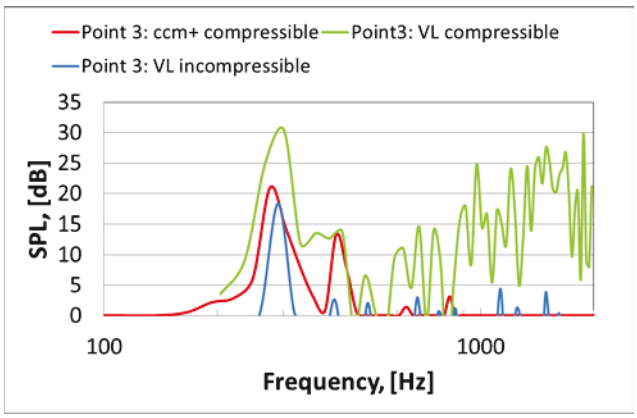

FIGURE 11: SPL spectra at point 3 for case 1: VL incompressible (blue); VL compressible (green); StarCCM+ compressible (red)

The results obtained in the StarCCM+ simulations are between both VL cases, though, the characteristic frequencies agree well. Although the peaks of the StarCCM+ results have a small displacement opposite to VL results. The major reason for these differences is on the one hand the different outlet boundary conditions used in these CFD simulations, and on the other hand in differences between Direct Computational Aeroacoustics and hybrid approach with separates generation and propagation of sound. Note, that in addition, StarCCM+ takes into account also the quadrupole sources. Figure 12 shows contribution of quadrupole term at point 2 for case 2. Here, the dipole surface sources p'_L in Eg. (8) and quadrupole volume sources p'_Q in Eg. (9) are separately loaded. Two peaks for level about 20 dB at 430 and 830 Hz are shown. For point 3 the effect of volume source was irrelevant.

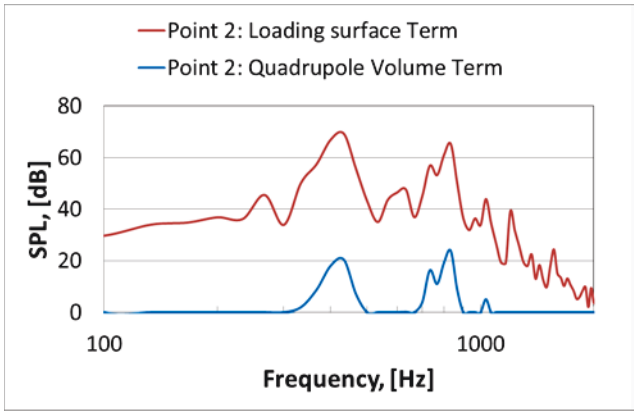

FIGURE 12: Surface and volume sources contribution at point 2 for case 2: dipole term (red); quadrupole term (blue)

Further, the SPL for different volume flux were investigated. In the Fig. 13, the FW-H spectra from OpenFOAM with VL and in Fig. 14 from StarCCM+ calculations are presented.

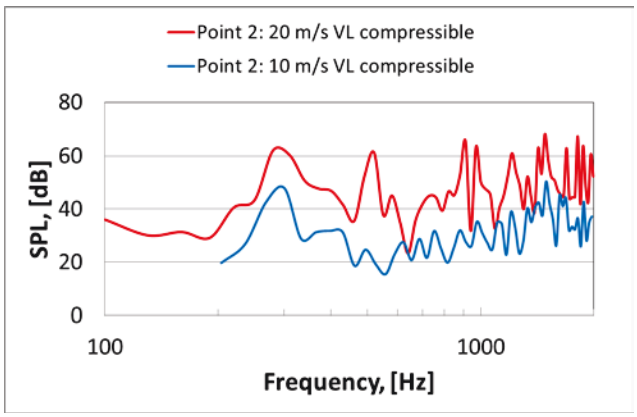

FIGURE 13: SPL spectra at Point 2 for case 1 (blue) and case 2 (red) obtained with OpenFOAM and VL

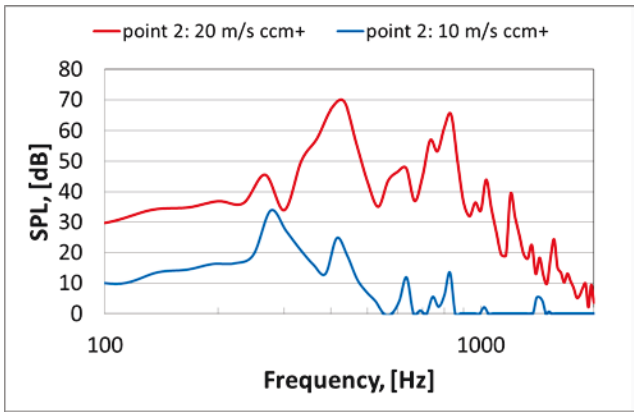

FIGURE 14: SPL spectra at Point 2 for case 1 (blue) and case 2 (red) obtained with StarCCM+

Both spectra reveal a small displacement in frequencies peaks. This can be explained with the higher turbulence intensity in case 2. Therefore, these two flows are not completely similar. The data comparison shows that the calculated SPL in case 2 (20 *m/s* at inlet) corresponds to the sound from passenger car at the distance of 10 *m*. In case 1 (10 *m/s* at inlet) SPL corresponds to sound from normal conversation at the distance of 1 *m*. The obtained Sound Level in case 1 is in accordance with the demanded comfort conditions while that of case 2 reveals a unpleasant sound strength. .

6. CONCLUSIONS

The presented work demonstrates that two different CAA approaches lead to similar predictions of the sound propagation. The comparison of the results of incompressible and compressible flow simulation further reveals, that compressibility effects have to be accounted for in the source region.

Virtual.Lab has advantages in calculation of the sound parameters in the far field. In contrast, StarCCM+ provides more details and accurate results in the flow domain. Note that both approaches create files of enormous size. For example, the OpenFOAM data set covering a time period of 0.1 *s* requires 800 *Gb* storage for the considered geometry. The only transient pressure data file of StarCCM+ has the size of 128 *Gb* for elapsed time of 0.15 *s*. Nevertheless, both Virtual.Lab and StarCCM+ allow to compute the sound generation and propagation in complicated geometries using a high-performance computer.

ACKNOWLEGMENTS

We thank Prof. F. Obermeier for helpful discussions and comments. The conversion of the OpenFOAM data in Ideas*.unv file has been realized with a program prepared by the Novicos GmbH. We acknowledge their support.

REFERENCES

[1] Lighthill, M., On Sound Generated Aerodynamically. Proc Roy. Soc. (London), **A 211**, 564-577, (1952).

[2] Curle, N., The Influence of Solid Boundaries on Aerodynamic Sound. Proc. Roy. Soc. (London), **A 231**, 505-514, (1955).

[3] Ffowcs Williams, J., Hawkings, D. Sound Generation by Turbulence and Surfaces in Arbitrary Motion. Phil. Trans. Roy. Soc. (London**), A 262**, 321-342, (1969).

[4] Möhring, W., Müller, E.-A., Obermeier, F., Schallerzeugung durch instationäre Strömung als singuläres Störungsproblem, Acustica **21**, (1969).

[5] Hirschberg, A., Rienstra, S., Theoretical Background: Aeroacoustics. Large Eddy Simulation for Acoustics, Cambridge Aerospace Series, Edited by C. Wagner, T. Hüttl, P. Sagaut, 24-88, (2007).

[6] Segaert, P., Die Randelemente-Metode (Boudary Element Method BEM): Möglichkeiten und Einschränkungen für die Anwendung in der Fahrzeugakustik. FKFS, Workshop Mess- und Analysetechnik in der Fahrzeugakustik, Stuttgart, 9.–10.10.2007, (2007).

[7] Caro, S., Manera, J., Toppinga, R., Mendonca, F., Validation of a New hybrid CAA Strategy and Application to the Noise Generated by a Flap in Simplified HVAC Duct. AIAA Paper 09-3352, (2009).

[8] Detry, S., Manera, J., Aero-acoustic Predictions of Industrial Dashboard HVAC Systems. Baltimore, Maryland NOISE-CON 2010, (2010).

[9] Obermeier, F., Konstantinov, M., Shishkin, A., Wagner, C., Sound Generation by Low Mach Number Flow through Pipes with Diaphragm Orifices. New Results in Numerical and Experimental Mechanics IX (STAB Symposium 2012). Springer Series: Notes on Numerical Fluid Mechanics and Multidisciplinary Design. ISSN: 1612-2909. (in print).